

Dynamical Properties of the Anderson Impurity Model within a Diagrammatic Pseudoparticle Approach

S. Kirchner

Department of Physics & Astronomy, Rice University, Houston, Texas 77005

J. Kroha

Physikalisches Institut, Universität Bonn, 53115 Bonn, Germany

P. Wölfle

Institut für Theorie der Kondensierten Materie, Universität Karlsruhe, 76128 Karlsruhe, Germany

The Anderson model of a twofold spin degenerate impurity level in the limit of infinite Coulomb repulsion, $U \rightarrow \infty$, coupled to one and two degenerate conduction bands or channels, is considered in pseudo-particle representation. We extend the Conserving T-Matrix Approximation (CTMA), a general diagrammatic approximation scheme based on a fully renormalized computation of two-particle vertex functions in the spin and in the charge channel, to the calculation of thermodynamic and spectral properties. In the single-channel case, the CTMA yields in the Kondo regime a temperature independent Pauli spin susceptibility for temperatures below the Kondo temperature T_K and down to the lowest temperatures considered, reproducing the exact spin screening in the Fermi liquid state. The impurity spectral density appears to remain non-singular down to the lowest temperatures, in agreement with Fermi liquid behavior. However, the unitarity sum rule, which is crucial for an impurity solver like the CTMA to be applicable within Dynamical Mean Field Theories for strongly correlated lattice models, is overestimated at the lowest temperatures. We argue that this shortcoming may be due to numerical imprecision and discuss an appropriate scheme for its correction. In the two-channel case, the spectral density calculated within CTMA exhibit qualitatively the correct non-Fermi liquid behavior at low temperatures, i.e. a powerlaw singularity.

PACS numbers: 71.10.-w, 71.27.+a, 71.28.+d, 71.55.-i, 71.45.-d

I. INTRODUCTION

Over the past two decades the problem of correlated electrons on a lattice has emerged as a central theme of condensed matter theory. With the exception of one-dimensional systems, there are no systematic analytical methods available for solving models like the Hubbard model. A powerful approximation scheme is the Dynamical Mean Field Theory, in which the lattice problem is mapped onto an effective single impurity Anderson model (SIAM), with self-consistently determined properties of the conduction electrons^{1,2}. It is a non-trivial task to solve these SIAMs. The properties of real Kondo or mixed valence impurities in metals are of interest in their own right, with recent emphasis on non-Fermi liquid behavior in multi-channel models^{3,4,5,6}. Various methods have been successfully applied to solve these models in certain parameter regimes. The Bethe ansatz (BA) method allows to calculate the thermodynamic properties of models with a flat conduction electron density of states^{7,8}. Bosonization methods have been used to obtain, for example, the finite-size spectrum of one- and two-channel impurities⁹. Conformal field theory is a powerful tool to analyze the low energy excitations of multi-channel models^{10,11,12}. The method of continuous unitary transformations¹³ has been successfully applied to the Kondo model in the vicinity of the Toulouse point¹⁴. These analytical methods are complemented by numerical methods like Quantum Monte Carlo

simulations (for not too low temperatures and moderate U)^{15,16,17} and Wilson's Numerical Renormalization Group (NRG) which has been very successful for not too large degeneracies in the spin or charge channel^{18,19,20}. The difficulty with quantum systems of the Anderson impurity type is the strong on-site Hubbard repulsion, which effectively constrains the quantum dynamics to a Hilbert space with fixed impurity occupation number and makes these problems inaccessible by straightforward perturbation theory. It is, in particular, difficult to describe the weak coupling (fluctuating local moment) behavior at high energies and the strong coupling fixed point behavior, realized below a strong coupling energy scale, typically the Kondo temperature T_K , by a single technique. In view of possible applications as an "impurity solver" within DMFT methods or to quantum impurity and quantum dot systems with a complex local spectrum, an accurate method which does not rely on integrability conditions or on the simplicity of the local or conduction electron spectrum is highly desirable. For that purpose we had proposed earlier a general diagrammatic approximation scheme²¹. The starting point is a pseudoparticle representation of the impurity level, where the constrained dynamics are built into the very definition of the quantum fields²², and approximations conserving its internal symmetry are defined by means of Luttinger-Ward functionals. The conserving approximation which incorporates the dominant, local spin and charge fluctuations on the level of a fully

renormalized calculation of the total two-particle vertex (or T-matrix) has been termed the Conserving T-Matrix Approximation (CTMA). In contrast to previous approximations like the Non-Crossing Approximation (NCA)^{23,24,25} and its extensions²⁶, the CTMA describes the weak as well as the strong coupling behavior of the single-channel SIAM correctly on the level of the pseudoparticle propagators^{21,27}. However, physically observable spectral properties had not yet been calculated because of their computational complexity.

In this article we present CTMA results for the thermodynamic and spectral properties of the $SU(N)\times SU(M)$ Anderson impurity model, N being the local spin degeneracy and M the number of identical, conserved conduction channels. We will focus on the single-channel Fermi liquid case ($N = 2$, $M = 1$), although results for the two-channel non-Fermi liquid sector of the model ($N = 2$, $M = 2$) will also be shown. The spin susceptibility as well as the frequency dependence of the impurity electron selfenergy indicate that the spin-screened Fermi liquid ground state of the $N = 2$, $M = 1$ SIAM is indeed captured by CTMA. However, the unitarity sum rule of the spectral density, which is vital for DMFT applications, is overestimated. A detailed inspection of the impurity electron selfenergy shows that this failure seems to originate from an imprecise treatment of high-energy processes, either due to numerical inaccuracy or due to CTMA neglecting non-singular potential scattering terms, and that such imprecision influences the low-energy behavior via the Kramers-Kronig relation. Based on this analysis we propose below a phenomenological correction scheme which imposes the causality of the impurity selfenergy, and which may thus make the CTMA applicable as an impurity solver for DMFT calculations. This approach amounts to adding an appropriate potential scattering term to the real part of the impurity selfenergy, taken to be a temperature independent constant. We will term this scheme the “effective potential scattering method”.

The paper is organized as follows. We describe the conserving pseudoparticle technique in section II, including several physical and technical justifications of the CTMA. The detailed CTMA self-consistent equations are given in the Appendix. The CTMA results for the temperature dependent, static spin susceptibility and for the impurity spectrum are presented in sections III and IV, respectively. Our effective potential scattering correction scheme is discussed in detail at the end of section IV. In section V, we compare the CTMA and NCA result for the spectral density of the two-channel SIAM, where the ground state is not a Fermi liquid. We conclude with a discussion of the results in section VI.

II. MODEL AND CONSERVING T-MATRIX APPROXIMATION

We consider the $SU(N)\times SU(M)$ SIAM in the limit of infinite Coulomb repulsion, implying that the N -fold degenerate impurity level (called d-level here), labeled by spin $\sigma = -N/2, \dots, +N/2$, is at most singly occupied. The empty impurity state is M -fold degenerate, labeled by $\bar{\mu} = 1, \dots, M$, and is coupled to a corresponding degenerate degree of freedom in the conduction band, e.g. z-component of angular momentum. In the pseudoparticle representation, the singly occupied (empty) level is created by fermionic (bosonic) operators f_σ^\dagger (b_μ^\dagger), which satisfy the constraint $Q = \sum_\sigma f_\sigma^\dagger f_\sigma + \sum_\mu b_\mu^\dagger b_\mu = 1$. The physical (or d) electron creation operator on the impurity site is $d_\sigma^\dagger = \sum_{\bar{\mu}} f_\sigma^\dagger b_{\bar{\mu}}$. The $SU(N)\times SU(M)$ Anderson impurity Hamiltonian is then defined by

$$H = \sum_{\vec{k}\sigma\mu} \epsilon_k c_{\vec{k}\sigma\mu}^\dagger c_{\vec{k}\sigma\mu} + \sum_\sigma \epsilon_{d,\sigma} f_\sigma^\dagger f_\sigma + V \sum_{\sigma\mu} (c_{0\sigma\mu}^\dagger b_\mu^\dagger f_\sigma + h.c.) + \lambda Q. \quad (1)$$

Here, $c_{0\sigma\mu}^\dagger = \sum_{\vec{k}} c_{\vec{k}\sigma\mu}^\dagger$ creates a conduction electron at the impurity site $\vec{R} = 0$ and $\epsilon_{d,\sigma} = \epsilon_d + \sigma g \mu_B B$ is the impurity level in a magnetic field B , with μ_B and g the Bohr magneton and the Landé factor, respectively. The operator b_μ transforms according to the conjugate representation of $SU(M)$. We denote the density of states (DOS) of the conduction electrons at the Fermi energy ϵ_F by $N(0)$ and assume it to be structureless. (All numerical results were obtained for a Gaussian DOS. Note, however, that our method works for arbitrarily structured DOS.) Instead of the hybridization V , we will frequently use $\Gamma = \pi N(0)V^2$ as a parameter of the model. In the Kondo regime, $\Gamma \ll \epsilon_d$ where the low energy excitations resemble those of the Kondo model, the above Hamiltonian has a dynamically generated strong coupling scale, the Kondo temperature T_K , where perturbation theory breaks down,

$$T_K = D \left(\frac{N\Gamma}{\pi D} \right)^{(M/N)} \exp \left(- \frac{\pi |\epsilon_d|}{N\Gamma} \right), \quad (2)$$

where $2D$ is the bandwidth of the conduction electron DOS. The Hamiltonian (1) possesses a $U(1)$ gauge symmetry with respect to simultaneous transformations of f_σ and b_μ related to the conserved charge Q , λ being the local gauge field. The exact projection of the dynamics onto the Hilbert subspace $Q = 1$ is accomplished by taking a gauge with a time independent λ , re-defining the zero of the energy scale as $\omega \rightarrow \omega + \lambda$, and letting $\lambda \rightarrow \infty$ in all expressions; see Ref. 28 and the appendix of Ref. 20 for details of the projection technique. The charge conservation in conjunction with the constraint $Q = 1$ implies an orthogonality catastrophe between the $Q = 1$ initial and the $Q = 0$ final states, and leads to

infrared threshold power-law behavior of the pseudoparticle Green's functions $G_{f,b}(\omega) \propto \omega^{-\alpha_{f,b}}$. In the Fermi liquid case, $M \leq N - 1$, the exponents $\alpha_{f,b}$ are closely related to the average impurity occupation number n_d via the Friedel sum rule^{29,30,31},

$$\alpha_f = (2n_d - n_d^2)/N \quad \alpha_b = 1 - n_d^2/N \quad (3)$$

Approximation schemes for calculating $G_{f,b}$ which violate the gauge symmetry would, hence, violate the orthogonality of initial and final states, and should be expected to give incorrect results for physical quantities, even though certain aspects of the Fermi liquid fixed point can be described by symmetry-breaking approximations^{32,33}. Therefore, we take great care to preserve the gauge symmetry. It can be reconciled with the time independent choice of the gauge field λ necessary for the $Q = 1$ projection by employing a conserving approximation, derived from a Luttinger-Ward generating functional Φ ^{34,35}. The local selfenergies Σ_α , $\alpha = f, b, c$, defined by

$$G_{f\sigma}^{-1}(\omega) = \omega - \epsilon_{d\sigma} - \lambda - \Sigma_f(\omega) \quad (4)$$

$$G_b^{-1}(\omega) = \omega - \lambda - \Sigma_b(\omega) \quad (5)$$

$$G_{c\sigma}^{-1}(\omega) = G_{c0\sigma}^{-1}(\omega) - \Sigma_{c\sigma}(\omega), \quad (6)$$

where $G_{c0\sigma}^{-1}(\omega) = \sum_{\vec{k}}(\omega - \epsilon_k)^{-1}$, are generated by functional differentiation of Φ with respect to the *self-consistently* renormalized Green's functions $\Sigma_\alpha(\omega) = \delta\Phi/\delta G_\alpha(\omega)$. As a result, for any given approximation to Φ a set of self-consistent nonlinear integral equations for Σ_f and Σ_b is obtained, which, in general, cannot be solved analytically but is amenable to numerical solution. The central task is then to find the correct generating functional which captures the essential physics of the problem at hand.

Non-Crossing Approximation (NCA). The NCA is often used for its computational simplicity to obtain a rough description, and it even captures the universal behavior inherent to Kondo-type problems³⁶. However, the NCA recovers the correct Kondo scale T_K only because of a fortunate compensation of the neglect of spin-flipping logarithmic terms and an incorrect logarithmic resummation of potential scattering terms^{37,38}. Below T_K it develops spurious infrared singularities in physical quantities. The NCA breaks down in a magnetic field B even in the weak coupling regime ($T > T_K$ and/or $B > T_K$), producing, in addition to the two Zeeman-split Kondo peaks a third, field independent resonance in the impurity spectral density at the Fermi energy. It seems that this spurious behavior originates from the incorrect treatment of the potential scattering in NCA mentioned above. On the level of auxiliary particles, the NCA does not give the correct FL threshold exponents Eq. (3), but instead $\alpha_f^{NCA} = M/(N + M)$, $\alpha_b^{NCA} = N/(N + M)$. It can be shown by power counting arguments, using $\alpha_f^{NCA} + \alpha_b^{NCA} = 1$, that any self-consistent calculation involving only a *finite* number of skeleton selfenergy diagrams just reproduces the incorrect NCA exponents.

Conserving T-Matrix Approximation (CTMA). Hence, selfenergies and two-particle vertex functions must be comprised of an *infinite* class of skeleton diagrams in order to describe the Fermi liquid fixed point. Since the latter is a consequence of the singlet formation between conduction electron and impurity spin, it is natural to assume that higher than two-particle correlations need not be considered in the single-channel case. The total vertex functions of conduction electrons (c) and local degrees of freedom (pseudofermions f , slave bosons b) are then two-particle T-matrices which are obtained from an infinite summation of irreducible parts via Bethe-Salpeter equations. We use the smallness of the pa-

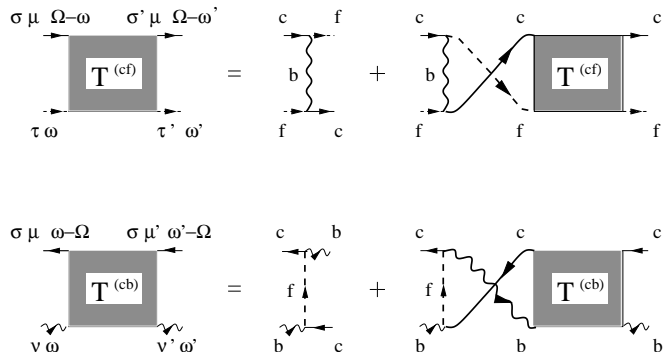


FIG. 1: Diagrammatic representation of the Bethe-Salpeter equations for the vertex functions $T^{(cf)}$ and $T^{(cb)}$ defining the CTMA. Dashed, wiggly, and solid lines represent here and in the following the renormalized pseudofermion, slave boson, and the local conduction electron propagators, respectively. The external lines are for clarity only and are not part of the vertices.

rameter $V N(0) \ll 1$ to select the leading diagrams of the irreducible parts. This results in the ladder approximation for the total two-particle vertices shown in Fig. 1. The Luttinger-Ward functional that generates by second functional differentiation the vertex functions of Fig. 1 is constructed by connecting the entry and exit points by Green's function lines and is shown diagrammatically in Fig. 2. The diagram containing two (renormalized) boson lines is not a skeleton, is already contained in the first (NCA) diagram via self-consistency, and, hence, is omitted. The conserving approximation obtained in this way has been called Conserving T-Matrix Approximation (CTMA). The self-consistent equations for the vertex functions and selfenergies to be solved are given explicitly in Appendix A. Note that the $f - c$ and the $b - c$ vertices in Figs. 1 and 2 describe spin and charge fluctuations, respectively. Therefore the CTMA should provide a good approximation not only in the Kondo, but also in the mixed valence and empty impurity regimes. On a more formal level, the CTMA can be justified both near the weak and near the strong coupling fixed points. Expanding, in the weak coupling regime, the CTMA in terms of *bare*, projected Green's functions ($B = 0$), $G_{f\sigma}^0(\omega) = 1/(\omega \pm i0)$, $G_b^0(\omega) = 1/(\omega + \epsilon_d \pm i0)$, it is seen

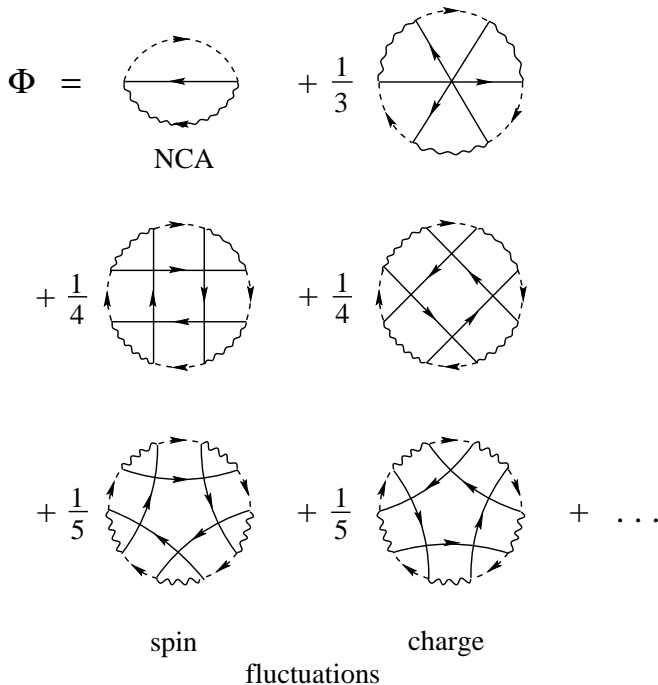


FIG. 2: Generating functional of the CTMA. The first diagram corresponds to the NCA generating functional. Each diagram contains exactly one closed auxiliary particle loop; diagrams with more than one such loop vanish after projection onto $Q = 1$. The class of CTMA diagrams beyond NCA is uniquely defined by the condition that each conduction electron line spans exactly two bare three-point hybridization vertices, as shown. The diagrams of the first and of the second column generate, by second functional derivative, $\delta^2\Phi/\delta G_c\delta G_f$ and $\delta^2\Phi/\delta G_c\delta G_b$, the spin and the charge fluctuation T-matrices, $T^{(cf)}$, $T^{(cb)}$, respectively (Fig. 1).

that the CTMA c-f vertex is exact up to leading logarithmic order, as seen in Fig. 3. Therefore, CTMA does incorporate the correct renormalization group (RG) flow in the weak coupling region³⁷. In particular, logarithmic potential scattering terms, present in each one of the diagrams of Fig. 3, cancel correctly when the two diagrams are added. Therefore, we expect that the CTMA correctly describes the Zeeman splitting of the Kondo resonance even in a large magnetic field, in contrast to the NCA, where only the first diagram of Fig. 3 is included, and its logarithmic potential scattering part leads to a spurious third peak at the the Fermi energy $\omega = 0$ (see above).

By virtue of the self-consistent inclusion of selfenergy diagrams in the propagators of Fig. 1 the CTMA vertex not only includes ladder but also parquet diagrams. Moreover, at any given order of *self-consistent* perturbation theory, the CTMA includes all diagrams with the maximum number of local spin and charge fluctuation processes in the sense of principal diagrams. Since these are expected to be responsible for the formation of the spin-singlet in the Kondo or mixed valence regime, CTMA

may be expected to capture the physics of the strong coupling fixed point of the single-channel SIAM as well. This will be shown by numerical evaluation in the following sections.

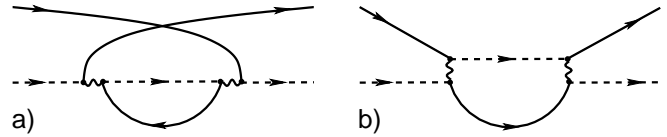


FIG. 3: Diagrams containing the leading logarithmic contributions to the c-f vertex function. In contrast to Figs. 1, 2, the lines represent the *bare* Green's functions here. a) Contribution from the NCA generating functional, b) additional contribution from the CTMA. Spurious logarithmic potential scattering terms cancel only when both terms are added. The c-b vertex has no logarithmic terms and, hence, does not flow under perturbative RG.

III. SPIN SUSCEPTIBILITY

In this section we report the CTMA result for the static impurity susceptibility

$$\chi_i(T) = \left. \frac{dM}{dB} \right|_{B=0} \quad (7)$$

of the $N = 2$, $M = 1$ SIAM in the Kondo regime and compare with NCA and Bethe ansatz results. Throughout the paper, the evaluations in this regime will be done for the typical parameter set $\epsilon_d/D = -0.81$, $\Gamma/D = 0.2$. In Eq. (7), yielding a low-temperature impurity occupation number of $n_{d\sigma} \simeq 0.47$ and $T_K = 4.16 \cdot 10^{-4}D$. Other parameter sets in the Kondo regime give similar results. $M = g\mu_B \sum_{\sigma} \sigma n_{\sigma}$ is the impurity magnetization,

$$n_{d\sigma} = \lim_{\lambda \rightarrow \infty} \frac{\int d\omega e^{-\beta\omega} \text{Im}G_{f\sigma}(\omega - i0)}{\int d\omega e^{-\beta\omega} \text{Im}[\sum_{\sigma} G_{f\sigma}(\omega - i0) + G_b(\omega - i0)]} \quad (8)$$

is the impurity occupation number with spin σ projected onto $Q = 1$ ^{20,28} ($\beta = 1/k_B T$), and the magnetic field B couples only to the impurity spin (Eq. (1)). The expression (7) is equivalent to the $\omega = 0$ limit of the causal dynamical linear response susceptibility

$$\chi_i(T, \omega = 0) = -i \int dt \Theta(t) \langle [\hat{M}(t), \hat{M}(0)] \rangle. \quad (9)$$

This is readily shown from Eqs. (7), (8), employing $d/dB = \sum_{\sigma} (dG_{f\sigma}/dB) \delta/\delta G_{f\sigma}$ and

$$\frac{dG_{f\sigma}}{dB} = G_{f\sigma}^2 \left[\sigma g\mu_B + \sum_{\sigma'} \frac{\delta\Sigma_{f\sigma}}{dG_{f\sigma'}} \frac{dG_{f\sigma'}}{dB} \right], \quad (10)$$

which follows from the definition of $G_{f\sigma}$.

$$\frac{\delta\Sigma_{f\sigma}}{dG_{f\sigma'}} = \gamma_{\sigma, \sigma'} \quad (11)$$

is the irreducible four-point pseudofermion vertex. Any conserving approximation by construction fulfills the equivalence of Eqs. (7) and (9), since it respects the Ward identity (11). We choose to use Eq. (7), because it is computationally less demanding than the correlation function Eq. (9).

Note that additional terms $\chi_b(T)$ and $\chi_{ib}(T)$ arise, if B couples also to the conduction electron spin. $\chi_b(T)$ is the constant Pauli susceptibility of the conduction band and $\chi_{ib}(T)$ a mixing term correlating the impurity and the conduction electron magnetization. Since the latter is, for a flat DOS, due to the electronic polarization at the bottom of the band, $\chi_{ib}(T)$ is usually negligible for $T \ll D$.

$\chi_i(T)$ is of principal interest as an indicator of whether CTMA captures the spin singlet Fermi liquid ground state of the single-channel SIAM. The result is shown in Fig. 4. While at exponentially high temperature, $\ln(T/T_K) \gg 1$, $\chi_i(T) = \mu_M^2/T$, typical for a free, fluctuating local moment, $\chi_i(T)$ shows T -independent Pauli behavior for $T \lesssim 0.1 T_K$ and down to the lowest T considered, characteristic for the completely spin-screened Fermi liquid state. By contrast, the low- T behavior of the NCA is a power law, $\chi_i^{NCA}(T) - \chi_i^{NCA}(0) \propto -T^{1/3}$. At $T = 0$, $\chi_i(T)$ acquires the value

$$\chi_i(0) = \frac{(g\mu_B)^2}{4T_L}, \quad (12)$$

which defines the universal low-temperature scale, T_L , of the Kondo or Anderson model, related to T_K by the Wilson number $W = T_K/T_L$.

The comparison of the CTMA result with exact methods like NRG¹⁸ or BA^{7,8,39} can be made quantitative. The dimensionless quantity $\bar{\chi}_i(T/T_K) = \chi_i(T)/(\mu_M^2/T_K)$ is known to be a universal function of T/T_K (i.e. independent of the microscopic parameters of the Hamiltonian), with $\bar{\chi}_i(0) = W$. Self-consistent approaches like NCA or CTMA reproduce this universality, since they include a resummation of the logarithmic terms of perturbation theory⁴⁰. In comparing the CTMA and the BA results one must, however, observe, that the breakdown scale of perturbation theory, T_K , depends on its precise definition. Therefore, care must be taken that the same definition of T_K is used for both, the CTMA and the exact method. In Wilson's original work on the Kondo model¹⁸, a Kondo temperature T_K^* was defined such that in the high temperature expansion of $\chi_i(T)$ all terms of $O(\ln(T/T_K^*)^{-2})$ cancel each other. Rasul and Hewson^{41,42,43} used the same criterion for the SIAM and found for the Kondo temperature,

$$T_K^* = \frac{1}{2\pi} \exp\left(1 + C - \frac{1}{2N}\right) \sqrt{\frac{D}{|\epsilon_d|}} T_K \quad (13)$$

where $C = 0.5772157$ is Euler's constant. With this definition, the universal Wilson number was found to be $W=0.4128$. Using the same definition, we find within

CTMA (Fig. 4),

$$W^{(CTMA)} = T_K^* \chi_i(0)/\mu_B^2 = 0.462. \quad (14)$$

In the BA method, T_K is defined in a somewhat different way due to a different cutoff scheme, resulting in a Wilson number $W^{BA} = \exp(C + 1/4)/\pi^{3/2} \approx 0.4107^{8,39}$ (for $N = 2$). Therefore, in the BA curve for $\bar{\chi}_i(T/T_K)$ we rescale T_K such that $\bar{\chi}_i(0)$ obtains Wilson's $T = 0$ value $W = 0.4128$ (Fig. 4). As seen from the figure, the CTMA result for the static susceptibility is in strikingly good quantitative agreement with the BA result not only for $T > T_K^*$, but also in the strong coupling region, $T \lesssim 0.1 T_K^*$. This shows that the CTMA describes the low-energy excitations around the Fermi liquid fixed point even quantitatively correctly at least in a thermodynamic quantity like the magnetic susceptibility. From the general properties of conserving approximations, one may expect the same to be true for dynamical quantities as well. This will be investigated in the next section.

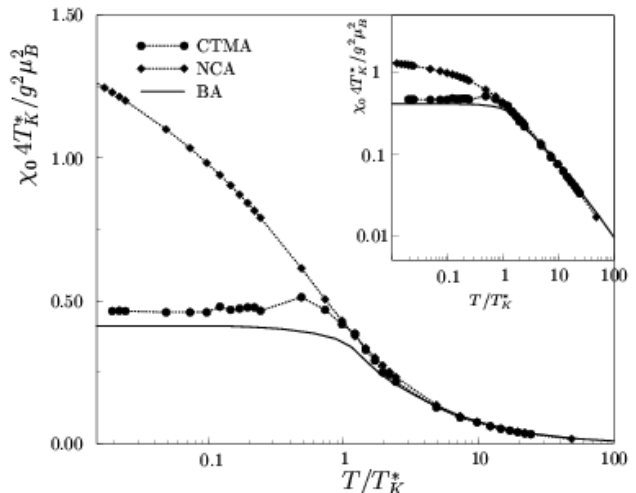


FIG. 4: The static magnetic susceptibility as a function of temperature. The temperature and the susceptibility scale are plotted in units of the conventional Kondo temperature T_K^* Eq. (13), that leads to the value $W = 0.4128$ for the Wilson number, see text. The CTMA curve agrees well with the exact BA result in both, the high temperature and in the strong coupling regimes, with only a small spurious intermediate maximum in the crossover region.

IV. DYNAMICAL PROPERTIES

The Pauli behavior of the impurity susceptibility calculated in the previous section shows that the spin structure of the low- T excitations captured by the CTMA free energy functional is such that it describes the complete screening of the impurity spin by the conduction electrons correctly even with good quantitative precision. It is the resulting absence of spin flip scattering at energies

below T_K that is responsible for the Fermi liquid behavior near the strong coupling fixed point of the single-channel Kondo or Anderson model. Therefore, one may conjecture, that the CTMA may capture the Fermi liquid nature of the low- T excitations as well, with well defined quasiparticles which should become visible in dynamical quantities like the impurity spectral density and the self-energy. This expectation is further supported by the fact that the CTMA does indeed reproduce the correct Fermi liquid threshold exponents on the level of the auxiliary particle dynamics²¹.

The quantities of prime interest for DMFT are the impurity electron Green's function,

$$G_{d\sigma}(\omega \pm i0) = \frac{1}{\omega + \epsilon_F - \epsilon_d \pm i\Gamma - \Sigma_{d\sigma}(\omega \pm i0)}, \quad (15)$$

and the interaction part of the selfenergy, $\Sigma_{d\sigma}(\omega)$, in the spin-screened case, $N = 2$, $M = 1$. The Fermi liquid theory implies certain exact low-energy properties, which the CTMA results must be compared to, namely the unitarity limit for the impurity spectral density at the Fermi level $\tilde{A}_{d\sigma}(0)$, the half width $\tilde{\Gamma}$ and position $\tilde{\epsilon}_d$ of the Kondo resonance, as well as the low-energy behavior of $\text{Im}\Sigma_{d\sigma}(\omega)$,

$$\tilde{A}_{d\sigma}(0) = \frac{\sin^2(\pi n_{d\sigma})}{\pi\Gamma}, \quad T = 0 \quad (16)$$

$$\tilde{\Gamma} = \frac{4}{\pi W} \sin^2(\pi n_{d\sigma}) T_K^* \quad (17)$$

$$\tilde{\epsilon}_d = \frac{2}{\pi W} \sin(2\pi n_{d\sigma}) T_K^* \quad (18)$$

$$\text{Im}\Sigma_{d\sigma}(\omega - i0) = a \Gamma \frac{\omega^2 + (\pi T)^2}{T_K^2} \quad (19)$$

$$a = \frac{\pi^4 W^2}{8e^{3/2+2C}} \frac{(R-1)^2}{\sin^2(\pi n_{d\sigma})} \frac{|\epsilon_d|}{D}, \quad (20)$$

where $R = 2$ is the Wilson ratio. The proof of these relations is compiled in Appendix B.

A. CTMA solution and Fermi liquid behavior

For the computation of $G_{d\sigma}(\omega)$ within the CTMA, observe that it is related to the single-particle conduction electron T-matrix, $t_{c\sigma}(\omega) = V^2 G_{d\sigma}(\omega)$, where, after projection onto $Q = 1$ only diagrams with a single pseudoparticle loop, i.e. irreducible diagrams, remain. In the conserving scheme it is, therefore, constructed as

$$G_{d\sigma}(\omega) = \frac{1}{V^2} \lim_{\lambda \rightarrow \infty} \frac{1}{Q(\lambda)} \frac{\delta\Phi}{\delta G_{c\sigma}(\omega)}. \quad (21)$$

The corresponding CTMA diagrams are shown in Fig. 5, and the details about their evaluation are given in Appendix A.

It is worth noting that, by definition, the impurity electron propagator is equivalent to the

$f - b$ “particle-hole” correlation function, $G_{d\sigma}(t) = -i\langle \hat{T} \{ b^\dagger(t) f_\sigma(t) f_\sigma^\dagger(0) b(0) \} \rangle$. This might seem to offer another possibility of calculating $G_{d\sigma}$ using the irreducible $f - b$ vertex $\Gamma_{fb} = \delta^2\Phi/\delta G_{f\sigma}\delta G_b$. However, any diagram of the $f - b$ particle-hole correlator constructed in this way contains necessarily two pseudoparticle loops, and, hence, vanishes by projection. Therefore, in CTMA the $f - b$ correlation function is comprised of the (NCA-like) $f - b$ bubble diagram only, which is clearly not sufficient to recover the Fermi liquid strong coupling fixed point. We note in passing that the non-trivial contributions to Γ_{fb} comprising the full G_d are generated from free energy diagrams which contain more than one pseudoparticle loop, but are not contained in CTMA. As a conclusion, in CTMA $G_{d\sigma}(\omega)$ must be calculated unambiguously using Eq. (21).

The CTMA results for the d-electron spectral function, $A_{d\sigma}(\omega) = \text{Im}G_{d\sigma}(\omega - i0)/\pi$ are shown in Figs. 6 and 7 for $T = T_K$ and $T = 0.01T_K$, respectively, together with its decomposition into the $f - b$ bubble contribution (1st diagram in Fig. 5) and the vertex corrections (2nd and 3rd diagrams in Fig. 5). Notably, even at elevated temperature, $T = T_K$, the vertex corrections are not negligible. For $T \rightarrow 0$ the $f - b$ bubble develops an infrared powerlaw divergence $\propto |\omega|^{\alpha_f + \alpha_b - 1}$. Since for our parameter set in the Kondo regime the exponent $\alpha_f + \alpha_b - 1 \approx 0.056$ is rather small, and the pseudoparticle exponents, Eq. 3, are obtained asymptotically, this singularity starts to develop for $T = 0.01T_K$ merely as a discontinuity in the slope of $A_{d\sigma}(\omega)$. Most importantly, however, the total d -electron spectral function does not show any infrared singularity on the scale of T , and the width $\tilde{\Gamma}$ and position $\tilde{\epsilon}_d$ of the Kondo resonance are in excellent agreement with the Fermi liquid predictions, Eqs. (17), (18), given the uncertainty in these quantities arising from the fact that the Kondo resonance deviates from the Lorentzian shape for $\omega > T_K$ (see Appendix B). In contrast, the unitarity limit, Eq. (16), is significantly violated in Fig. 7. To investigate the origin of this failure, we plot in Fig. 8 the imaginary part of the interaction selfenergy $\Sigma_{d\sigma}(\omega - i0)$. It is seen that even at the lowest temperature the CTMA result does not develop any singularity, in contrast to NCA. However, the position of the minimum of $\text{Im}\Sigma_{d\sigma}(\omega - i0)$ is incorrectly shifted to a negative frequency ω_0 of $O(T_K)$,

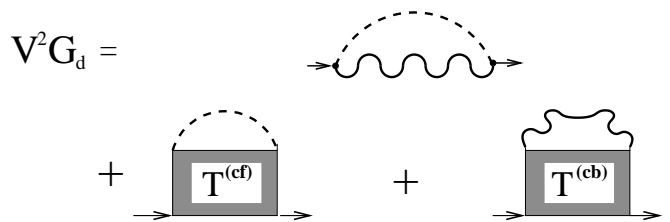


FIG. 5: Diagrams defining the d-electron Green's function within CTMA. For details of their evaluation see Appendix A.

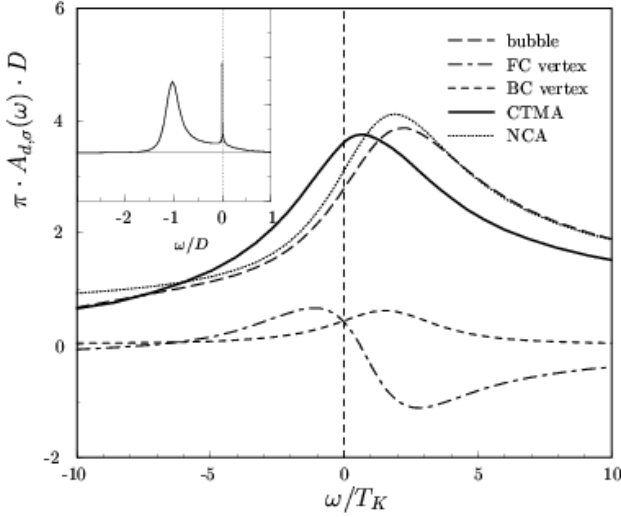


FIG. 6: CTMA and NCA results for the local spectral density $A_{d\sigma}(\omega)$ for $\epsilon_d/D = -0.81$, $\Gamma/D = 0.2$ at $T = T_K = 6.16 \cdot 10^{-4}D$. The decomposition of the CTMA result into $f-b$ bubble and vertex corrections arising from $T^{(cf)}$ (fc vertex) and $T^{(cb)}$ (bc vertex) is also shown. The NCA shows an incorrectly large shift of the Kondo peak of $O(T_K)$ towards positive frequencies, which is corrected by CTMA, see text.

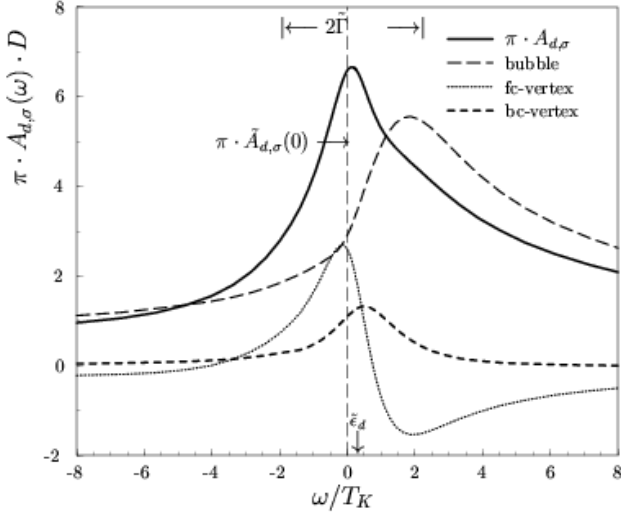


FIG. 7: CTMA impurity spectral function and decomposition into $f-b$ bubble and vertex contributions for the same parameters as in Fig. 6, but at $T = 0.01T_K$. The exact values for $A_{d\sigma}(0)$, $\tilde{\Gamma}$, $\tilde{\epsilon}_d$, Eq. (16), (17), (18), are displayed for comparison.

where $\text{Im}\Sigma_{d\sigma}(\omega_0 - i0)$ acquires a spurious negative value. Even at the lowest T considered, $\text{Im}\Sigma_{d\sigma}(\omega - i0)$ shows $(\omega - \omega_0)^2$ behavior for $|\omega - \omega_0| \lesssim T_K$ (Fig. 8). Its prefactor,

determined from our parameter set from Fig. 9 as $0.0244 D$, is in excellent agreement with the exact Fermi liquid value, $a\Gamma = 0.0239 D$ (Eqs. (19), (20)). The temperature dependence of the minimum of $\text{Im}\Sigma_{d\sigma}(\omega - i0)$ is analyzed in Fig. 10. Again, the CTMA solution shows T^2 behavior from the lowest T considered up to $T \simeq T_K$, $\text{Im}\Sigma_{d\sigma}(\omega_0 - i0) = \tilde{a}\Gamma(\pi T/T_K)^2$, where the prefactor $\tilde{a}\Gamma = 0.013 D$ is of the same order of the exact value $\tilde{a}\Gamma$, although roughly a factor of 2 too small.

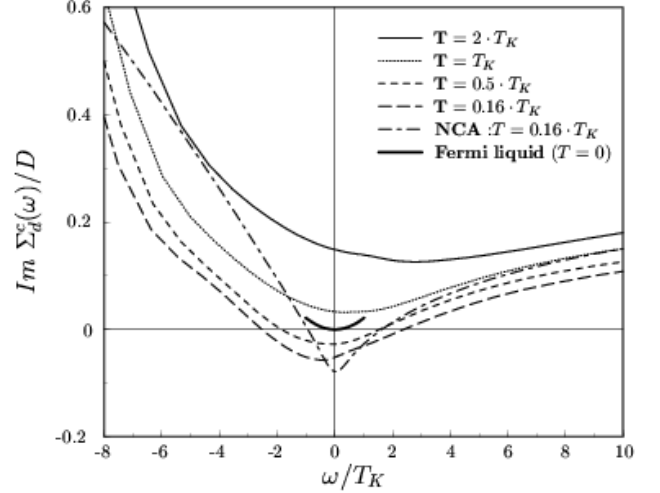


FIG. 8: Correlation part of the physical d -electron selfenergy $\text{Im}\Sigma_{d\sigma}(\omega)$ calculated in CTMA for various temperatures and $\epsilon_d/D = -0.81$, $\Gamma/D = 0.2$. For the lowest temperature shown, $T = 0.16 \cdot T_K$, the NCA result (dot-dashed line) is shown for comparison, showing the cusp-like infrared singularity typical for NCA. The bold solid line centered at the origin represents the $T = 0$ behavior expected for our parameter set based on Fermi liquid theory, Eqs. (19), (20).

To summarize our analysis, the ω^2 , T^2 behavior of the impurity electron selfenergy, which stems from the low-energy excitations and is at the heart of the Fermi liquid theory, is even quantitatively reproduced by the CTMA without spurious singularities. However, the location of this minimum at $\omega = 0$ and the exact unitary value $A_{d\sigma}(0)$ of the impurity spectral density are not reproduced. The latter is crucial to avoid a non-causal behavior of the correlation part of the impurity selfenergy $\Sigma_{d\sigma}(\omega)$ and, hence, for an application as an impurity solver within DMFT². $\Sigma_{d\sigma}^{tot}(\omega - i0) = i\Gamma + \Sigma_{d\sigma}(\omega - i0)$, as well as the location of this minimum at $\omega = 0$, As will be discussed below in more detail, both of these failures can be attributed to an incorrect treatment of non-singular potential scattering processes at high energies, $\omega \gg T_K$. We will propose a corresponding correction scheme in the next subsection.

We conclude the present subsection by considering briefly another test case of Fermi liquid behavior, the empty orbital regime. In this case the d -electron density of states consists of only one broadened, unoccupied

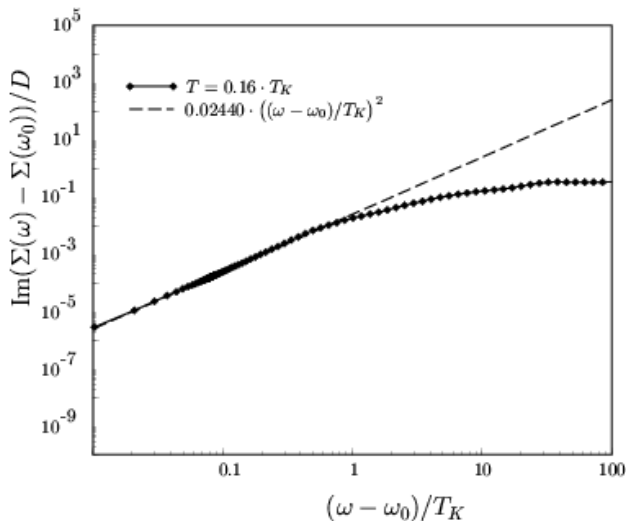


FIG. 9: Log-log plot of $\text{Im} \Sigma_{d\sigma}(\omega - i0) - \text{Im} \Sigma_{d\sigma}(\omega_0 - i0)$ versus frequency, $(\omega - \omega_0)/T_K$, for $T = 0.16 T_K$. ω_0 is the position of the minimum of $\text{Im} \Sigma_{d\sigma}(\omega - i0)$ in Fig.8. The dashed line is the fit to the low-frequency quadratic behavior of $\text{Im} \Sigma_{d\sigma}(\omega - i0)$ and represents the function $y = 0.02440(\omega - \omega_0)^2/T_K^2$, see text.

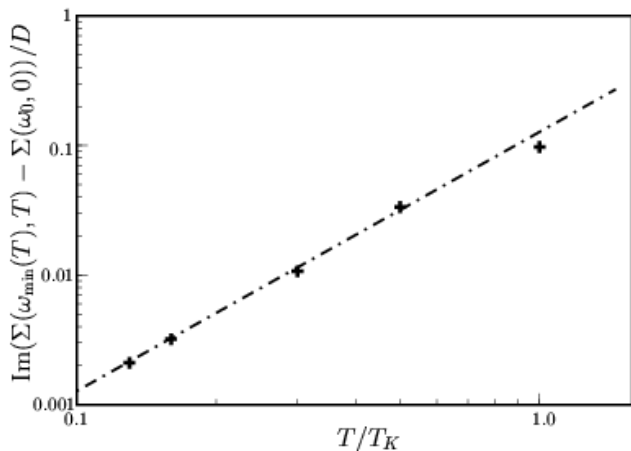


FIG. 10: Log-log plot of the minimum value of the imaginary part of the selfenergy, $\text{Im} \Sigma_{d\sigma}(\omega = \omega_{\min}(T), T) - \text{Im} \Sigma_{d\sigma}(\omega = \omega_0, T = 0.01T_K)$ versus T/T_K . $\omega_{\min}(T)$ is the position of the minimum for a given temperature T , see Fig. 8. Quadratic in T behavior is clearly visible for $T \lesssim T_K$. The dashed line is given by $y = 0.013 D \cdot (\pi T/T_K)^2$.

single-particle resonance at a renormalized impurity level $\epsilon_d > 0$ far above the Fermi energy. In the pseudoparticle representation, the empty-impurity case is still a non-trivial strongly correlated problem because of the operator constraint $Q = 1$. Fig. 9 shows the NCA and the CTMA spectral density for $\epsilon_d/D = +0.81$, $\Gamma/D = 0.2$. NCA is well known to fail badly in this case, producing a spurious, singular peak at $\omega = 0$, which arises from the X-ray-like divergences of the pseudoparticle Green's

functions. In the CTMA solution, the vertex corrections tend to cancel the infrared peak of the $f - b$ bubble. Presumably, the wiggles visible in the CTMA spectrum are due to numerical imprecision, but may also be due to a systematically imperfect cancellation of infrared divergent terms. In any case, the CTMA does not produce any definite peak structure at $\omega = 0$, significantly improving the description of the Fermi liquid behavior in the empty orbital regime.

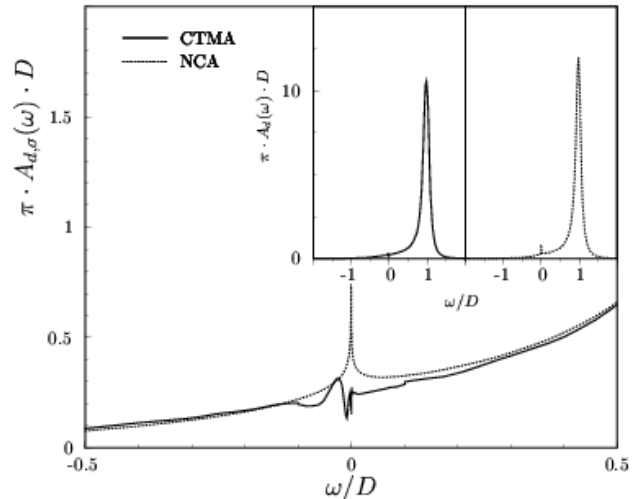


FIG. 11: CTMA (solid line) and NCA (dotted line) result for the local spectral density in the empty impurity regime, $\epsilon_d/D = +0.81$, $\Gamma/D = 0.2$ for $T = 1.0 \cdot 10^{-4} D$. The resulting occupation per spin is $n_{d\sigma} = 0.037$. The insets show the CTMA (left panel) and the NCA (right panel) spectral functions over the complete band width.

B. Effective potential scattering correction

Within the pseudoparticle technique, it is a non-trivial task to separate the single-particle hybridization part $i\Gamma$, of the total impurity selfenergy, from the interaction contribution, $\Sigma_{d\sigma}(\omega)$, since the hybridization is an interaction term in this representation, Eq. (1). Hence, while the auxiliary particle method is designed for a systematical treatment of the low-energy spin scattering processes, it is difficult to accurately calculate the non-singular potential scattering part of the total impurity selfenergy

$$\Sigma_{d\sigma}^{\text{tot}}(\omega) = \omega + \epsilon_F - \epsilon_d - G_{d\sigma}(\omega)^{-1} \quad (22)$$

$$= i\Gamma + \Sigma_{d\sigma}(\omega), \quad (23)$$

which involves hybridization processes at high energies of order ϵ_d . Technically speaking, the $\omega = 0$ value of $\text{Im} \Sigma_{d\sigma}^{\text{tot}}(\omega)$ is influenced by both, the real and the imaginary part of $G_{d\sigma}(0)$, and hence by the high-energy features of the spectrum through the Kramers-Kronig relation. Obtaining the precise values of the real and imag-

inary parts of $\Sigma_{d\sigma}^{tot}(0 - i0)$ would therefore require calculating the high-energy features of the local spectrum to a precision better than $\sim T_K$. Clearly, this is a formidable task, both with respect to numerical precision and to diagrammatical systematics: Since any potential scattering term gives a non-singular, energy independent contribution to $\Sigma_{d\sigma}^{tot}(0)$, it is unlikely that a class of principal diagrams can be identified that reproduces the correct value. On the other hand, the class of CTMA diagrams does describe the correct ω^2, T^2 behavior, reflecting the correct low-energy many-body dynamics.

Based on these considerations, we propose a simple, phenomenological scheme to incorporate the correct potential scattering contributions. It amounts to adding an appropriate *frequency and temperature independent* constant $\Delta\epsilon$ to the *real part* of $\Sigma_{d\sigma}^{tot}(\omega)$. It has the effect of shifting the zero of the frequency scale in *all* quantities, and in particular in $\text{Im}\Sigma_{d\sigma}(\omega)$, by virtue of the self-consistency.⁴⁴ Therefore, $\Delta\epsilon$ can be chosen such that at $T = 0$ the minimum of $\text{Im}\Sigma_{d\sigma}(\omega - i0)$ is obtained at $\omega = 0$ in accordance with Fermi liquid behavior, Eq. (19). In the CTMA solution the position of the minimum of $\text{Im}\Sigma_{d\sigma}(\omega)$ does not significantly change with temperature for $T \lesssim 0.2T_K$, see Fig. 8, as expected from the Fermi liquid behavior, Eq. (19). Hence, we have determined $\Delta\epsilon$ from the solution at $T = 0.16T_K$ to fulfill the Fermi liquid condition above. The results for the impurity spectral function corrected in this way is displayed for various T in Fig. 12. It shows accurate agreement

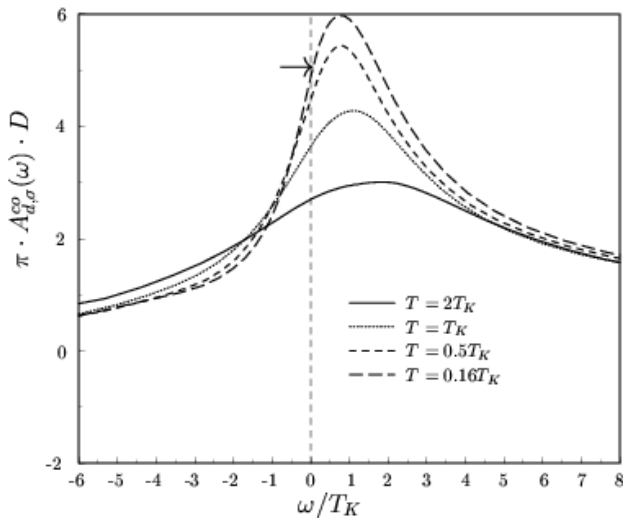


FIG. 12: CTMA spectral functions with a constant potential scattering term added to the real part of $\Sigma_{s\sigma}(\omega - i0)$ according to the effective potential scattering method, see text. No low-energy singularity occurs, and the unitarity limit (arrow) is accurately fulfilled at the lowest temperatures.

with the unitarity limit, even though this was not directly implied by our adjustment procedure. This can be seen as a further indication that CTMA correctly cap-

tures the Fermi liquid dynamics of the problem, missing only part of the potential scattering contributions. The corresponding imaginary part of the total impurity selfenergy, Eq. (22), is shown in Fig. 13. Again, the Fermi liquid behavior, Eq. (19), is well obeyed. The minimum value of $\text{Im}\Sigma_{d\sigma}^{tot}(\omega - i0)$ approaches for $T \rightarrow 0$ the value $\Gamma_{eff} \approx 0.139D$ instead of the exact limit $\Gamma = 0.2D$. As discussed above, we attribute this to an inaccurate treatment of single-particle hybridization processes within CTMA. Note however, that for the DMFT algorithm² only the interaction part $\Sigma_{d\sigma}(\omega)$ of the self-energy is important. In the auxiliary particle method it is obtained from the impurity Green function by the subtraction $\Sigma_{d\sigma}(\omega - i0) = \Sigma_{d\sigma}^{tot}(\omega - 0) - i\Gamma_{eff}$, where Σ^{tot} is given by Eq. (22), and its imaginary part remains strictly non-negative.

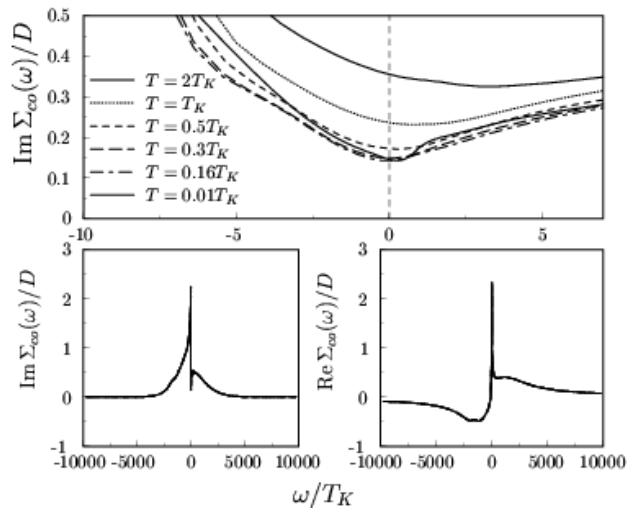


FIG. 13: Real and imaginary part of the total impurity selfenergy $\Sigma_{d\sigma}^{tot}(\omega - i0)$, corrected by the effective potential scattering method. The curvature of $\text{Im}\Sigma_{d\sigma}^{tot}(\omega - i0)$ at the Fermi energy does not change considerably from $T = 0.16T_K$ down to $T = 0.01T_K$. The small bump in the curve for $T = 0.01T_K$ at positive ω is attributed to numerical inaccuracy. At $\omega = 0, T \rightarrow 0$, $\text{Im}\Sigma_{d\sigma}^{tot}(0 - i0)$ assumes the effective hybridization $\Gamma_{eff} \approx 0.139D$, somewhat smaller than the exact value $\Gamma = 0.2D$. Γ_{eff} is to be subtracted from $\text{Im}\Sigma_{d\sigma}^{tot}(\omega - i0)$ in order to obtain the interaction part of the local selfenergy.

V. TWO-CHANNEL KONDO BEHAVIOR

To complete the discussion of dynamical quantities we calculate the local spectral function of the two-channel ($N = 2, M = 2$) Anderson model. Here the low-temperature fixed point is of a distinct non-Fermi liquid nature¹⁰, involving a non-vanishing zero-point entropy, $S(0) = k_B \ln \sqrt{2}$, and a logarithmic divergence of the static susceptibility, $\chi(T) \propto -\ln T/T_K$, signaling a non-

degenerate ground state and over-screening of the local spin, respectively^{11,45}.

For the two-channel Kondo (2CK) model, the effective low-energy model of the two-channel SIAM, it has been shown using conformal field theory⁴⁶ that the local spectrum has a cusp at the Fermi level, $A^{2CK}(\omega) - A^{2CK}(0) \propto -|\omega|^{1/2}$. The weight of this power law becomes asymmetrical for $\omega > 0$ and $\omega < 0$, when the particle-hole symmetry is broken, e.g., by an additional potential scattering term. This weight asymmetry is analogous to the shift of the Kondo resonance $\tilde{\epsilon}_d$ in the single-channel case. Extrapolating the Fermi liquid results of Appendix B to the two-channel SIAM, the weight asymmetry may be expected to be of $O(T_K/\epsilon_d)$. Very recently, the auxiliary particle threshold exponents for the two-channel Anderson model have been calculated using the Bethe ansatz.⁴⁷ It was shown that the exponents, like in the single-channel case, are functions of the local valence.

The Bethe ansatz solution shows that the 2CK ground state involves intricate correlations between both conduction channels and the local spin. Thus, one would expect that in a diagrammatic treatment three-particle correlation functions are needed, and that CTMA, which involves only two-particle T -matrices, is not able to capture the correct 2CK ground state. Indeed, in the multi-channel ($M \geq 2$) case NCA as well as CTMA give incorrect, valence independent auxiliary particle threshold exponents as given in Section II⁴⁸. Surprisingly, however, NCA correctly reproduces qualitatively the leading low-energy singularities of physical quantities like the susceptibility⁴⁸ or the local density of states.⁶ In Fig. 14 we show the CTMA solutions for the impurity spectral function of the two-channel SIAM in comparison to the NCA result, both showing a $|\omega|^{1/2}$ cusp. The cusp of the NCA curve has a strong weight asymmetry, which is presumably an overestimation, like in the Fermi liquid case (Fig. 6). This is significantly improved by the CTMA solutions. However, as mentioned above, we believe that a systematical description of the 2CK behavior would require an extension of the CTMA to include three-particle correlation functions.

VI. SUMMARY

To conclude, we have extended the analysis of the Conserving T-Matrix Approximation to thermodynamical and dynamical properties. It had been demonstrated earlier that for the single-channel Anderson impurity model the CTMA captures the correct spin-screened Fermi liquid ground state on the level of the auxiliary particle dynamics, signaled by the Fermi liquid exponents of the auxiliary particle propagators for all fillings²¹. In the present work we have shown that the CTMA also describes the Fermi liquid strong coupling behavior of physical quantities correctly. It is, thus, the first diagrammatic method that captures both the low-energy Fermi liquid behavior and the high-temperature properties of

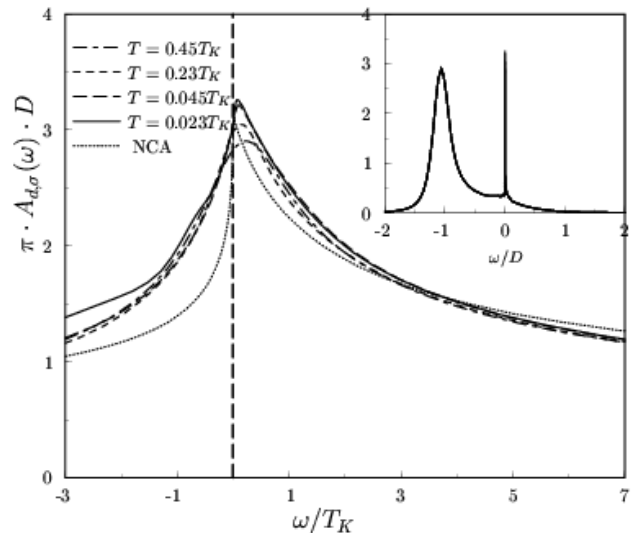


FIG. 14: CTMA results for the impurity spectral density of the two-channel SIAM, with $\epsilon_d = -0.81 D$ $\Gamma = 0.2 D$ at various temperatures. The NCA result is shown for comparison. The $|\omega|^{1/2}$ cusp develops at the Fermi level, with a weight asymmetry due to potential scattering. The inset shows the spectrum over a wider frequency range.

quantum impurity problems of the single-channel Anderson model type on the same footing. In particular the CTMA describes the static spin susceptibility in the Kondo regime correctly for all temperatures. The Wilson number obtained within CTMA is in striking agreement with the exact one. We also showed, that the physical d-electron spectral density in the single-channel case ($N = 2$, $M = 1$) is able to mend most of the deficiencies of the NCA in the Kondo and empty orbital regime of the model. Especially, no spurious infrared singularities occur. The deviation of the CTMA solution from the exact unitarity limiting value for the spectral density at the Fermi level could be traced back to an insufficiently accurate treatment of high energy potential scattering processes. To correct this deficiency, we have proposed a phenomenological method by adding an appropriate, effective potential scattering term $\delta\epsilon$ to the real part of the impurity selfenergy, and defining an effective single-particle hybridization rate Γ_{eff} . As a result, all essential Fermi liquid properties are fulfilled without spurious non-causal behavior. Future directions will be on one hand to develop the CTMA as an impurity solver within DMFT, and on the other hand to explore the applicability of the CTMA to more complicated quantum impurity problems, which may exhibit a Fermi liquid instability due to, e.g., a quantum critical point, or in a magnetic field.

Acknowledgments

It is a pleasure to acknowledge stimulating discussions with J. Brinckmann, T. A. Costi, and Q. Si. We thank T. A. Costi for numerous helpful suggestions. S. Kirchner acknowledges support by the Deutsche Forschungsgemeinschaft and NSF Grant No. DMR-0090071. Additional support has been provided by SFB 195 and by SFB 608 of the DFG.

APPENDIX A: CTMA EQUATIONS

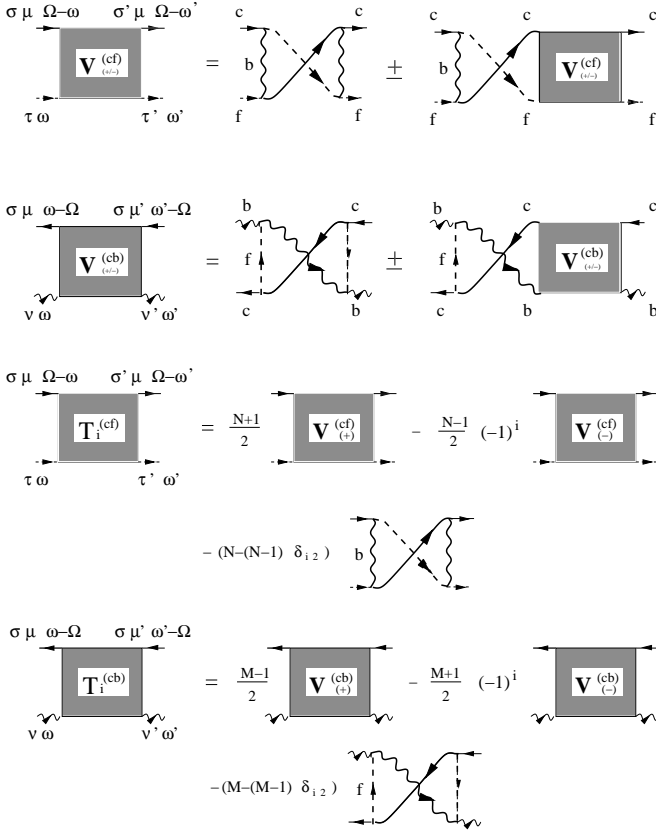


FIG. 15: Diagrammatic representation of the integral equations comprising the T-matrices that enter in the expressions for the auxiliary particle selfenergies, see text for details.

In the following we present a compilation of the CTMA equations which determine the imaginary part of the impurity propagator G_d , the auxiliary particle selfenergies Σ_f and Σ_b and the basic building block of the CTMA, i.e. the analytically continued 4-point vertices $T^{(cf)}$ and $T^{(cb)}$. Due to the fact that the first diagram in Fig.1 does not lead to a proper vertex contribution, we start the summation with the two-rung diagram. In order to include the proper channel and spin summations with enter even-rung and odd-rung diagrams differently, it is necessary to solve for the ladders with alternating signs as

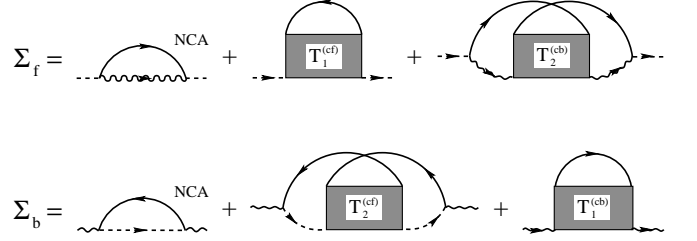


FIG. 16: Auxiliary particle selfenergies Σ_f and Σ_b : The first diagram is the NCA contribution, where however fully CTMA-renormalized Green functions have to be used. The second and third diagram constitute the vertex corrections from $T^{(fc)}$ and $T^{(bc)}$.

well. As already mentioned in the main text the two-rung diagrams, that is the inhomogeneous parts $I^{(cf)}$ and $I^{(cb)}$ of Eqs. A1 and A2 lead to selfenergy contributions which are already included in the NCA. Hence, in order to avoid over-counting these non-skeletons have to be subtracted before calculating the selfenergies. The resulting equations are diagrammatically depicted in Fig.15. We label the external frequencies of the 4-point vertices $V^{(cf)}$ and $V^{(cb)}$ such, that the first (second) argument denotes the in- (out-)going frequency of the pseudo particle propagator and the third frequency labels the center of mass-frequency propagating through the ladder, see Fig. 15. On the Matsubara frequencies, the vertex functions are therefore given by

$$\begin{aligned}
 V_{\sigma,\tau}^{(cf)\mu(\pm)}(i\omega_n, i\omega'_n, i\Omega_n) &= I_{\sigma,\tau}^{(cf)\mu}(i\omega_n, i\omega'_n, i\Omega_n) \pm \frac{\Gamma}{\pi N(0)} \frac{1}{\beta} \sum_{\omega''_n} G_{b\bar{\mu}}(i\omega_n + i\omega''_n - i\Omega_n) \times \\
 &\quad G_{f\sigma}(i\omega''_n) G_{c\mu\tau}^0(i\Omega_n - i\omega''_n) V_{\tau,\sigma}^{(cf)\mu(\pm)}(i\omega''_n, i\omega'_n, i\Omega_n), \\
 I_{\sigma,\tau}^{(cf)\mu}(i\omega_n, i\omega'_n, i\Omega_n) &= -\left(\frac{\Gamma}{\pi N(0)}\right)^2 \frac{1}{\beta} \sum_{\omega''_n} G_{b\bar{\mu}}(i\omega_n + i\omega''_n - i\Omega_n) G_{f\sigma}(i\omega''_n) G_{c\mu\tau}^0(i\Omega_n - i\omega''_n) G_{b\bar{\mu}}(i\omega'_n + i\omega''_n - i\Omega_n),
 \end{aligned} \tag{A1}$$

and

$$\begin{aligned}
V_{\mu,\nu}^{(cb)(\pm)\sigma}(i\omega_n, i\omega'_n, i\Omega_n) &= I_{\mu,\nu}^{(cb)\sigma}(i\omega_n, i\omega'_n, i\Omega_n) \pm \frac{\Gamma}{\pi N(0)} \frac{1}{\beta} \sum_{\omega''_n} G_{f\sigma}(i\omega_n + i\omega''_n - i\Omega_n) \times \\
&\quad G_{b\bar{\mu}}(i\omega''_n) G_{c\nu\sigma}^0(i\omega''_n - i\Omega_n) V_{\nu,\mu}^{(cb)(\pm)\sigma}(i\omega''_n, i\omega'_n, i\Omega_n), \\
I_{\mu,\nu}^{(cb)\sigma}(i\omega_n, i\omega'_n, i\Omega_n) &= -\left(\frac{\Gamma}{\pi N(0)}\right)^2 \frac{1}{\beta} \sum_{\omega''_n} G_{f\sigma}(i\omega_n + i\omega''_n - i\Omega_n) \times G_{b\bar{\mu}}(i\omega''_n) G_{c\nu\sigma}^0(i\omega''_n - i\Omega_n) G_{f\sigma}(i\omega'_n + i\omega''_n - i\Omega_n).
\end{aligned} \tag{A2}$$

After analytical continuation to the real axis the T-matrices obey the following linear Fredholm integral

equations of the second kind:

$$\begin{aligned}
V_{\sigma,\tau}^{(cf)(\pm)\mu}(\omega, \omega', \Omega) &= I_{\sigma,\tau}^{(cf)(\pm)\mu}(\omega, \omega', \Omega) \pm (-\Gamma) \int \frac{d\varepsilon}{\pi} f(\varepsilon - \Omega) \times \\
&\quad G_{b\bar{\mu}}(\omega + \varepsilon - \Omega) G_{f\sigma}(\varepsilon) A_{c\mu\tau}^0(\Omega - \varepsilon) V_{\tau,\sigma}^{(cf)(\pm)\mu}(\varepsilon, \omega', \Omega) \\
I_{\sigma,\tau}^{(cf)(\pm)\mu}(\omega, \omega', \Omega) &= \frac{\Gamma^2}{\pi N(0)} \int \frac{d\varepsilon}{\pi} f(\varepsilon - \Omega) \times G_{b\bar{\mu}}(\omega + \varepsilon - \Omega) G_{f\sigma}(\varepsilon) A_{c\mu\tau}^0(\Omega - \varepsilon) G_{b\bar{\mu}}(\omega' + \varepsilon - \Omega)
\end{aligned} \tag{A3}$$

and

$$\begin{aligned}
V_{\mu,\nu}^{(cb)(\pm)\sigma}(\omega, \omega', \Omega) &= I_{\mu,\nu}^{(cb)(\pm)\sigma}(\omega, \omega', \Omega) \pm (+\Gamma) \int \frac{d\varepsilon}{\pi} f(\varepsilon - \Omega) \times \\
&\quad G_{f\sigma}(\omega + \varepsilon - \Omega) G_{b\bar{\mu}}(\varepsilon) A_{c\nu\sigma}^0(\varepsilon - \Omega) V_{\nu,\mu}^{(cb)(\pm)\sigma}(\varepsilon, \omega', \Omega) \\
I_{\mu,\nu}^{(cb)(\pm)\sigma}(\omega, \omega', \Omega) &= -\frac{\Gamma^2}{\pi N(0)} \int \frac{d\varepsilon}{\pi} f(\varepsilon - \Omega) \times G_{f\sigma}(\omega + \varepsilon - \Omega) G_{b\bar{\mu}}(\varepsilon) A_{c\nu\sigma}^0(\varepsilon - \Omega) G_{f\sigma}(\omega' + \varepsilon - \Omega).
\end{aligned} \tag{A4}$$

In order to simplify the expressions for the selfenergies $\Sigma_{f,\sigma}$ and Σ_b it proves useful to introduce

with

$$\begin{aligned}
T_1^{(cf)} &= \frac{N+1}{2} V^{(cf)(+)} + \frac{N-1}{2} V^{(cf)(-)} - N I^{(cf)}, & \Sigma_{f\sigma}^{(NCA)}(\omega) &= M\Gamma \sum_{\mu} \int \frac{d\varepsilon}{\pi} f(-\varepsilon) A_{c\mu\sigma}^0(\varepsilon) G_{b\bar{\mu}}(\omega - \varepsilon) \\
T_2^{(cf)} &= \frac{N+1}{2} V^{(cf)(+)} - \frac{N-1}{2} V^{(cf)(-)} - I^{(cf)}, & \Sigma_{b\bar{\mu}}^{(NCA)}(\omega) &= N\Gamma \sum_{\sigma} \int \frac{d\varepsilon}{\pi} f(\varepsilon) A_{c\mu\sigma}^0(\varepsilon) G_{f\sigma}(\omega + \varepsilon)
\end{aligned}$$

and

$$\begin{aligned}
T_1^{(cb)} &= \frac{M-1}{2} V^{(cb)(+)} + \frac{M+1}{2} V^{(cb)(-)} - M I^{(cb)}, \\
T_2^{(cb)} &= \frac{M-1}{2} V^{(cb)(+)} - \frac{M+1}{2} V^{(cb)(-)} - I^{(cb)}.
\end{aligned}$$

Then we obtain for the analytically continued advanced ($i\omega \rightarrow \omega - i0 \equiv \omega$) selfenergies:

$$\Sigma_{f\sigma}(\omega) = \Sigma_{f\sigma}^{(NCA)}(\omega) + \Sigma_{f\sigma}^{(cf)}(\omega) + \Sigma_{b\bar{\mu}}^{(cb)}(\omega) \tag{A5}$$

$$\Sigma_{b\bar{\mu}}(\omega) = \Sigma_{b\bar{\mu}}^{(NCA)}(\omega) + \Sigma_{b\bar{\mu}}^{(cf)}(\omega) + \Sigma_{b\bar{\mu}}^{(cb)}(\omega) \tag{A6}$$

$$\begin{aligned}
\Sigma_{f\sigma}^{(cf)}(\omega) &= M \int \frac{d\varepsilon}{\pi} f(\varepsilon - \omega) A_c^0(\varepsilon - \omega) \times \\
&\quad \pi N(0) T_1^{(cf)}(\omega, \omega, \varepsilon), \\
\Sigma_{f\sigma}^{(cb)}(\omega) &= -M \Gamma \int \frac{d\varepsilon}{\pi} \int \frac{d\varepsilon'}{\pi} f(\varepsilon - \omega) f(\varepsilon' - \omega) \times \\
&\quad A_c^0(\omega - \varepsilon) G_b(\varepsilon) \pi N(0) T_2^{(cb)}(\varepsilon, \varepsilon', \varepsilon + \varepsilon' - \omega) \times \\
&\quad A_c^0(\omega - \varepsilon') G_b(\varepsilon'),
\end{aligned}$$

and

$$\begin{aligned}\Sigma_{b\bar{\mu}}^{(cf)}(\omega) &= -N \Gamma \int \frac{d\varepsilon}{\pi} \int \frac{d\varepsilon'}{\pi} f(\varepsilon - \omega) f(\varepsilon' - \omega) \times \\ &\quad A_c^0(\varepsilon - \omega) G_f(\varepsilon) \pi N(0) T_2^{(cf)}(\varepsilon, \varepsilon', \varepsilon + \varepsilon' - \omega) \times \\ &\quad A_c^0(\varepsilon' - \omega) G_f(\varepsilon'), \\ \Sigma_{b\bar{\mu}}^{(cb)}(\omega) &= -N \int \frac{d\varepsilon}{\pi} f(\varepsilon - \omega) A_c^0(\omega - \varepsilon) \times \\ &\quad \pi N(0) T_1^{(cb)}(\omega, \omega, \varepsilon),\end{aligned}$$

where the vertex functions follow from $T_{1/2}^{(cf)}$ and $T_{1/2}^{(cb)}$ after performing the frequency summations and analytical continuation of the external frequencies. In the contour integrals around conduction line cuts we have used $A_c^0(\omega) = \frac{1}{\pi} \text{Im} G_{c\mu\sigma}^0(\omega - i0)/N(0)$.

Once the pseudo particle Green functions have been self-consistently calculated, physical properties can be determined. In order to construct the local Green function from the basic building block of our theory, the 4-point vertices $T^{(cf)}$ and $T^{(cb)}$, we note that the Bethe-Salpeter equations above yield either fully advanced or fully retarded T-matrices,

$$\begin{aligned}T^{RRR}(\omega, \omega', \Omega) &\equiv \quad \quad \quad (A7) \\ T(i\omega \rightarrow \omega + i0, i\omega' \rightarrow \omega' + i0, i\Omega \rightarrow \Omega + i0)\end{aligned}$$

or

$$\begin{aligned}T^{AAA}(\omega, \omega', \Omega) &\equiv \quad \quad \quad (A8) \\ T(i\omega \rightarrow \omega - i0, i\omega' \rightarrow \omega' - i0, i\Omega \rightarrow \Omega - i0)\end{aligned}$$

The local spectral density however requires the deter-

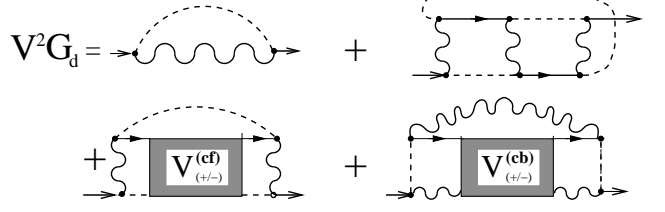


FIG. 17: Diagrammatic representation of the equation for the local d-electron Green function. The first diagram is the NCA contribution. As described in the text, because of the analytical structure of the Adsigma it is necessary to multiply with a rung at each end of the vertex functions $V_{(\pm)}^{(cf)}$, $V_{(\pm)}^{(cb)}$, as shown in the last two diagrams on the right-hand side. Hence the sum of these diagrams contains at least 4 rungs, i.e. the three-rung term must be added separately (second diagram on the right-hand side.)

mination of $T^{RRR}(\omega, \omega', \Omega)$. Therefore, its calculation is more involved. We construct $T^{RRR}(\omega, \omega', \Omega)$ by adding two rungs to each of the diagrams in $T^{(cf)}$ and $T^{(cb)}$. This then turns for example the two-rung diagram into a four-rung ladder. In order to include all contributing diagrams, it is then necessary to employ the T-matrices $V_{(\pm)}^{(cf)}$ and $V_{(\pm)}^{(cb)}$ instead of $T^{(cf)}$ and $T^{(cb)}$ and, in addition, the three-rung diagram has to be added, see Fig. 17. The equation for the advanced spectral function after projection onto the physical subspace then follows as

$$\begin{aligned}A_{d,\sigma}(\omega) &= A_{d,\sigma}^{(\text{NCA})}(\omega) + \frac{N(0)}{\pi^2 \Gamma} \left[\int_{-\infty}^{\infty} d\tilde{\varepsilon} \frac{e^{-\beta\tilde{\varepsilon}}}{f(\omega)} \int_{-\infty}^{\infty} d\varepsilon_1 \int_{-\infty}^{\infty} d\varepsilon_2 f(\varepsilon_1 - \tilde{\varepsilon}) f(\varepsilon_2 - \tilde{\varepsilon}) A_{c\sigma\mu}^0(\tilde{\varepsilon} - \varepsilon_1) A_{c\sigma\mu}^0(\tilde{\varepsilon} - \varepsilon_2) \cdot \right. \\ &\quad \text{Im} \{ G_{f\sigma}(\varepsilon_1) G_{f\sigma}(\varepsilon_2) G_b(\varepsilon_1 + \varepsilon_2 - \tilde{\varepsilon}) \} \cdot \text{Im} \{ G_{f\sigma}(\tilde{\varepsilon} - \omega) G_b(\varepsilon_1 - \omega) G_b(\varepsilon_2 - \omega) \} \\ &\quad + \int_{-\infty}^{\infty} d\tilde{\varepsilon} \frac{e^{-\beta\tilde{\varepsilon}}}{f(\omega)} \int_{-\infty}^{\infty} d\varepsilon_1 \int_{-\infty}^{\infty} d\varepsilon_2 f(\varepsilon_1 - \tilde{\varepsilon}) f(\varepsilon_2 - \tilde{\varepsilon}) A_{c\sigma\mu}^0(\tilde{\varepsilon} - \varepsilon_1) A_{c\sigma\mu}^0(\tilde{\varepsilon} - \varepsilon_2) \cdot \\ &\quad \text{Im} \{ G_{f\sigma}(\varepsilon_1) G_{f\sigma}(\varepsilon_2) \left[\frac{N-1}{2} \cdot V_{+, \sigma, \sigma'}^{cf}(\varepsilon_1, \varepsilon_2, \tilde{\varepsilon}) + \frac{N+1}{2} \cdot V_{-, \sigma, \sigma'}^{cf}(\varepsilon_1, \varepsilon_2, \tilde{\varepsilon}) \right] \} \cdot \\ &\quad \left. \text{Im} \{ G_{f\sigma}(\tilde{\varepsilon} - \omega) G_{b\bar{\mu}}(\varepsilon_1 - \omega) G_{b\bar{\mu}}(\varepsilon_2 - \omega) \} \right] \quad (A9) \\ &\quad + \int_{-\infty}^{\infty} d\tilde{\varepsilon} \frac{e^{-\beta\tilde{\varepsilon}}}{f(-\omega)} \int_{-\infty}^{\infty} d\varepsilon_1 \int_{-\infty}^{\infty} d\varepsilon_2 f(\varepsilon_1 - \tilde{\varepsilon}) f(\varepsilon_2 - \tilde{\varepsilon}) A_{c\sigma\mu}^0(\varepsilon_1 - \tilde{\varepsilon}) A_{c\sigma\mu}^0(\varepsilon_2 - \tilde{\varepsilon}) \cdot \\ &\quad \text{Im} \{ G_{b\bar{\mu}}(\varepsilon_1) G_{b\bar{\mu}}(\varepsilon_2) \cdot \left[\frac{M-1}{2} \cdot V_{+, \sigma, \sigma}^{cb}(\varepsilon_1, \varepsilon_2, \tilde{\varepsilon}) + \frac{M+1}{2} \cdot V_{-, \sigma, \sigma}^{cb}(\varepsilon_1, \varepsilon_2, \tilde{\varepsilon}) \right] \} \cdot \\ &\quad \left. \text{Im} \{ G_{b\bar{\mu}}(\tilde{\varepsilon} + \omega) G_{f\sigma}(\varepsilon_1 + \omega) G_{f\sigma}(\varepsilon_2 + \omega) \} \right],\end{aligned}$$

with

$$A_{d,\sigma}^{(\text{NCA})}(\omega) = \int d\varepsilon e^{-\beta\varepsilon} [A_{f\sigma}(\omega + \varepsilon) A_{b\bar{\mu}}(\varepsilon) - A_{f\sigma}(\varepsilon) A_{b\bar{\mu}}(\varepsilon - \omega)]. \quad (A10)$$

APPENDIX B: FERMI LIQUID RELATIONS

In this appendix we compile some exact Fermi liquid properties for the d-electron Green's function ($N = 2$,

$M = 1$),

$$G_{d\sigma}(\omega \pm i0) = \frac{1}{\omega + \varepsilon_F - \varepsilon_d \pm i\Gamma - \Sigma_{d\sigma}(\omega \pm i0)}. \quad (B1)$$

The interaction contribution $\Sigma_{d\sigma}(\omega \pm i0)$ to the selfenergy obeys the Fermi liquid relations

$$\text{Im}\Sigma_{d\sigma}(\omega \pm i0) = a \frac{\omega^2 + (\pi T)^2}{T_K^2}, \quad \omega, T \lesssim T_K \quad (\text{B2})$$

$$\int_{-\infty}^0 d\omega \frac{\partial \Sigma_{d\sigma}}{\partial \omega} G_{d\sigma}(\omega) = 0, \quad T = 0 \quad (\text{B3})$$

$$(\text{B4})$$

These imply the Friedel sum rule, $n_{d\sigma}(0) = \delta_\sigma$, with $n_{d\sigma}(0)$ the impurity occupation at $T = 0$ and δ_σ the scattering phase at the Fermi energy ϵ_F ,

$$\cot \delta_\sigma = \frac{\text{Re}G_{d\sigma}(0)}{\text{Im}G_{d\sigma}(0 + i0)}. \quad (\text{B5})$$

$$(\text{B6})$$

The impurity spectral density at the Fermi energy $\omega = 0$, $T = 0$ follows from Eqs. (B1), (B2), (B5) as

$$A_{d\sigma} = \frac{1}{\pi} \text{Im}G_{d\sigma}(0 - 0) = \frac{\sin^2(\pi n_{d\sigma})}{\pi \Gamma}. \quad (\text{B7})$$

The Fermi liquid relations also determine the width $\tilde{\Gamma}$, position $\tilde{\epsilon}_d$, and spectral weight z of the Kondo resonance. Using the quasiparticle weight $z = (1 - \partial \Sigma_{d\sigma} / \partial \omega|_{\omega=0})^{-1}$, the Green's function can be written for $|\omega|, T \lesssim T_K$,

$$G_{d\sigma}(\omega \pm i0) = \frac{z}{\omega - \tilde{\epsilon}_d \pm i\tilde{\Gamma}}, \quad (\text{B8})$$

with $\tilde{\epsilon}_d = z[\epsilon_F + \epsilon_d + \text{Re}\Sigma_{d\sigma}(0)]$, $\tilde{\Gamma} = z\Gamma$. z can be expressed in terms of the strong coupling parameters of the

Anderson model by equating the $T = 0$ spin susceptibility, Eq. (12), with the Pauli susceptibility of a Fermi liquid of quasiparticles with weight z , $\chi(0) = (g\mu_B)^2 A_{d\sigma}/z$,

$$z = \frac{4T_K^* \sin^2(\pi n_{d\sigma})}{\pi \Gamma W}, \quad (\text{B9})$$

and hence,

$$\tilde{\Gamma} = \frac{4}{\pi W} \sin^2(\pi n_{d\sigma}) T_K^*. \quad (\text{B10})$$

Combining Eqs. (B5), (B8), (B10) the position of the Kondo resonance relative to ϵ_F is given by

$$\tilde{\epsilon}_d = \frac{2}{\pi W} \sin(2\pi n_{d\sigma}) T_K^*. \quad (\text{B11})$$

The exact prefactor a of the quadratic behavior of $\text{Im}\Sigma_{d\sigma}(\omega)$ has been calculated for the Anderson model using direct perturbation theory to infinite order in the on-site repulsion U ^{49,50,51}. One obtains at $T = 0$, $\partial^2 \text{Im}\Sigma_{d\sigma}(\omega - i0) / \partial \omega^2 = \pi |\gamma(0,0)|^2 [A_{d\sigma}(0)]^3$, where $\gamma(0,0)$ is the full, local 2-electron vertex function at the Fermi energy and at $T = 0$. Using a Ward identity⁴⁹, it can be related to the quasiparticle density of states $A_{d\sigma}(0)/z$ and expressed as $\gamma(0,0) = (R - 1)/[z A_{d\sigma}(0)]$, where $R = 2$ is the Wilson ratio. Hence, taking into account Eq. (13), we obtain for the prefactor in Eq. (B2),

$$a = \frac{\pi^4 W^2}{8e^{3/2+2C}} \frac{(R-1)^2}{\sin^2(\pi n_{d\sigma})} \frac{|\epsilon_d|}{D}. \quad (\text{B12})$$

¹ W. Metzner and D. Vollhardt, Phys. Rev. Lett. **62**, 324 (1989).
² A. Georges, G. Kotliar, W. Krauth, and M. Rozenberg, Rev. Mod. Phys. **68**, 13 (1996).
³ M. Garnier, K. Breuer, D. Purdie, M. Hengsberger, Y. Baer, and B. Delley, Phys. Rev. Lett. **78**, 4127 (1997).
⁴ H. Ott, H. Rudigier, Z. Fisk, and J. Smith, Phys. Rev. Lett. **50**, 1595 (1983).
⁵ D. Cox, Phys. Rev. Lett. **59**, 1240 (1987).
⁶ D. Cox and A. Zawadowski, Adv. Phys. **47**, 599 (1998).
⁷ A. Tsvetick and P. Wiegmann, Adv. Phys. **32**, 453 (1983).
⁸ N. Andrei, K. Furuya, and J. H. Lowenstein, Rev. Mod. Phys. **55**, 331 (1983).
⁹ G. Zaránd and J. von Delft, Phys. Rev. B. **61**, 6918 (2000).
¹⁰ P. Nozières and A. Blandin, J. Phys. **41**, 193 (1980).
¹¹ A. Ludwig and I. Affleck, Phys. Rev. Lett. **67**, 3160 (1991).
¹² I. Affleck, A. Ludwig, H. Pang, and D. Cox, Phys. Rev. B **45**, 7918 (1992).
¹³ F. Wegner, Ann. Phys. (Leipzig) **3**, 77 (1994).
¹⁴ W. Hofstetter and S. Kehrein, Phys. Rev. B **63**, 140402 (2001).
¹⁵ J. Hirsch and R. Fye, Phys. Rev. Lett. **56**, 2521 (1986).
¹⁶ J. E. Gubernatis, J. E. Hirsch, and D. J. Scalapino,

Phys. Rev. B **35**, 8478 (1987).
¹⁷ J. E. Gubernatis, Phys. Rev. B **36**, 394 (1987).
¹⁸ K. Wilson, Rev. Mod. Phys. **47**, 773 (1975).
¹⁹ T. A. Costi, A. C. Hewson, and V. Zlatić, J. Phys. C **6**, 2519 (1994).
²⁰ T. A. Costi, J. Kroha, and P. Wölfle, Phys. Rev. B **53**, 1850 (1996).
²¹ J. Kroha, P. Wölfle, and T. A. Costi, Phys. Rev. Lett. **79**, 261 (1997).
²² S. Barnes, J. Phys. F: Met. Phys. **6**, 1375 (1976).
²³ Y. Kuramoto, Z. Phys. B **53**, 37 (1983).
²⁴ E. Müller-Hartmann, Z. Phys. B **57**, 281 (1984).
²⁵ N. Bickers, Rev. Mod. Phys. **59**, 845 (1987).
²⁶ F. B. Anders and N. Grewe, Europhys. Lett. **26**, 551 (1994).
²⁷ T. Schauerte, J. Kroha, and P. Wölfle, Phys. Rev. B. **62**, 4394 (2000).
²⁸ S. Kirchner, *Conserving T-Matrix Approach to Quantum Impurities with Application to Quantum Point Contacts* (Shaker, Aachen, 2002).
²⁹ B. Menge and E. Müller-Hartmann, Z. Phys. B **73**, 225 (1988).
³⁰ T. A. Costi, P. Schmitteckert, J. Kroha, and P. Wölfle,

- Phys. Rev. Lett. **73**, 1275 (1994).
- ³¹ T. A. Costi, P. Schmitteckert, J. Kroha, and P. Wölfle, Physica C **235**, 2287 (1994).
- ³² N. Read and D. Newns, J. Phys.C: Solid State Phys. **16**, L1055 (1983).
- ³³ D. E. Logan, M. P. Eastwood, and M. A. Tusch, J. Phys.C: Solid State Phys. **10**, 2673 (1998).
- ³⁴ G. Baym and L. Kadanoff, Phys. Rev. **124**, 287 (1961).
- ³⁵ G. Baym, Phys. Rev. **127**, 1391 (1962).
- ³⁶ N. E. Bickers, D. L. Cox, , and J. W. Wilkins, Phys. Rev. B **36**, 2036 (1987).
- ³⁷ S. Kirchner and J. Kroha, Journ. Low Temp. Phys. **126**, 1233 (2002).
- ³⁸ E. Lebanon, A. Schiller, and V. Zevin, Phys. Rev. B **64**, 245338 (2001).
- ³⁹ N. Andrei and C. Destri, Phys. Rev. Lett. **52**, 364 (1984).
- ⁴⁰ A. Rosch, J. Kroha, and P. Wölfle, Phys. Rev. Lett. **87**, 156802 (2001).
- ⁴¹ A. C. Hewson and J. W. Rasul, J. Phys.C: Solid State Phys. **16**, 6799 (1983).
- ⁴² J. W. Rasul and A. C. Hewson, J. Phys.C: Solid State Phys. **17**, 2555 (1984).
- ⁴³ J. W. Rasul and A. C. Hewson, J. Phys.C: Solid State Phys. **17**, 3337 (1984).
- ⁴⁴ Note that $\Delta\epsilon$ is analogous to a chemical potential. Since the shift $\Delta\epsilon \approx T_K \ll \epsilon_d, \Gamma$, and the impurity occupation $n_{d\sigma}$ is predominantly determined by the single-particle resonance at $\omega \approx \epsilon_d$, the resulting change of $n_{d\sigma}$ is of $O(T_K/[\Gamma(1 + (\epsilon_d/\Gamma)^2)])$, i.e. negligibly small.
- ⁴⁵ N. Andrei and A. Jerez, Phys. Rev. Lett **74**, 4507 (1995).
- ⁴⁶ I. Affleck and A. Ludwig, Phys. Rev. B **48**, 7297 (1993).
- ⁴⁷ H. Johannesson, N. Andrei, and C. J. Bolech, Phys. Rev. B **68**, 075112 (2003).
- ⁴⁸ Kirchner, unpublished.
- ⁴⁹ A. C. Hewson, *The Kondo Problem to Heavy Fermions* (Cambridge University Press, Cambridge, 1993).
- ⁵⁰ K. Yamada, Prog. Theor. Phys. **55**, 1345 (1976).
- ⁵¹ K. Yosida, Phys. Rev. **147**, 223 (1966).